

**Research Paper**

Introducing a New Method in Data Visualization: Stress Field Mapping in the Zagros Makran Transition Zone, Southern Iran

Shahrokh Pourbeyranvand

Assistant Professor, Seismological Research Center, International Institute of Earthquake Engineering and Seismology (IIEES), Tehran, Iran, beyranvand@iiees.ac.ir

Received: 21/01/2023

Revised: 24/02/2023

Accepted: 01/03/2023

ABSTRACT

This study introduces a new method for visualizing vector data for the first time. This method is based on RGB, attributing each rectangular cell within a grid with a specific square mesh size. Two different quantities are introduced, namely unidirectional and bidirectional, which will be illustrated using the two color circle types, 1 and 2, as color scales. Seeking the correct illustration of the directions with a color scale, the opposite directions (maximum horizontal stress direction or SHmax as an example) should be of the same color, making the problem more sophisticated so that the usual color wheel cannot be used. As an example, the SHmax variations in the Zagros Makran transition zone were mapped by using this new approach. Maximum horizontal stress directions are extracted from available earthquake focal mechanism data. The results show important variations in stress direction, which reflect the complicated tectonic environment of the study area. Several anomalies in the direction of SHmax are observed in the study area for the first time by implementing the proposed new method. Some of the anomalies take place in the areas where deeper earthquakes occur. This may imply the decoupling between the shallow seismogenic zone within the sedimentary cover and the crystalline basement, which is responsible for deeper events.

Keywords:

Direction; Earthquake focal mechanism; Stress; Tectonic; Visualization; Zagros Makran transition zone

1. Introduction

Many achievements have been accomplished in color theory from early works by Sir Isaac Newton, from whom the color circle, which we will refer to as type 1, stemmed from his works; up to recent progress in this area of science with the aid of newly developed modern computer systems (Shevell, 2003). However, the illustration of the direction-dependent or vector data is not a task as easy and intuitive to do as it seems. The concept of a color wheel or color circle can be a potential solution to this problem, but it has not been implemented yet. Furthermore, as we will see, this is not the correct answer to many issues, especially

the example we will discuss in this paper.

To progress in this issue, we first need to classify the direction-dependent quantities under discussion into two groups, unidirectional and bidirectional. Unidirectional quantities can be defined as direction-dependent quantities whose azimuth can vary from 0 to 360 degrees around the circle. On the other hand, bidirectional quantity is a direction-dependent quantity in which its azimuth equals its azimuth +/- 180 degrees. The latter case introduces a symmetrical nature as we witness in many direction-dependent data as stress or strain.

For the illustration of unidirectional data, it is enough to use the color wheel, introduced in the relevant references before but not yet used as a basis for visualizing vector data directions. The so-called unidirectional data can be visualized using the well-known color wheel, as we will see in the afterward sections of this paper. But the visualization of bidirectional vector data requires some innovation. A new color circle with a new RGB combination scheme is necessary for this purpose and will be addressed in this paper.

The Zagros Makran transition zone is located between two important seismotectonic zones of Iran many geophysical quantities vary on different sides of the Strait of Oman, including magnetic fabrics as an example (Bakhtari et al., 1998) and also the seismicity and depth of earthquakes. Thus, the stress field in this zone has been studied before because of the complexity of the tectonic environment and the importance of this area due to socioeconomic development in recent years (e.g., Pourbeyranvand, 2020). However, this study is new since the method of obtaining the stress directions is different compared to previous studies. In those previously published studies, the SH_{max} (maximum horizontal stress direction) was obtained by the inversion of a cluster of earthquake focal mechanisms. But in the present study, every single earthquake focal mechanism is a source of data and the stress information is derived from P , B or T axis depending on the mechanism of faulting as explained in the method section. The visualization of the stress field is accomplished for the first time in the present study, which exhibits some unseen anomalies in this area.

In the following sections, we will review the tectonic setting of the Zagros Makran transition zone to emphasize the importance of stress studies in this seismo-structurally complicated zone. Then the seismicity and earthquakes in the region will be discussed and stress information from single focal mechanism data will be extracted. Then the new method of visualization of vector data direction is proposed and the method is implemented. Finally, the results will be interpreted regarding the seismotectonics of the region and new aspects of the problem at hand will be investigated.

2. Tectonic Setting of the Study Area

Many great earthquakes have occurred in Iran, causing many casualties and considerable damage. Meanwhile, advances in civil, mining, and petroleum engineering over the past century have led to the development of stress measurement technologies. In geosciences, it is essential to gain knowledge about the stress field to understand the development of folded structures and the motion on faults that cause earthquakes. In the middle of the convergence between the Arabian and Eurasian plates, the north-northeast movement of the Arabian plate relative to Eurasia changes from 18 to 25 mm per year from west to east along the Zagros. The pole of this rotation is in North Africa (Walpersdorf et al., 2006). According to GPS studies, the north-south shortening varies from 9 mm/yr in the southeastern parts to about 4 mm/yr in the northwestern parts of the Zagros (Vernant et al., 2004; Masson et al., 2005; Raeesi et al., 2016). Thus, knowing about stress variations in Iran is necessary to study the deformation resulting from the oblique collision between the Eurasian and the Arabian plates and gain insight into the complicated tectonics of the region.

The Zagros Mountains extend from the Eastern Anatolian Fault in Turkey to the Makran Subduction in southern Iran. Due to the incredible complexity of this orogenic region and its importance in the convergence of the Arabian and Eurasian plates and the resulting deformations, many studies have been conducted in this region (e.g. Regard et al., 2010). Because superficial rupture with seismic activity is rare in the area, most of the information available about active faults in this region is derived from earthquakes (Talebian & Jackson, 2004). Earthquakes are usually difficult to attribute to a specific fault due to a thick sedimentary cover of about 10-14 km (Pirouz et al., 2017) (McQuarrie, 2004). Seismicity in the Zagros is distinguished from other regions of Iran by a large number of small seismic events.

The Zagros is one of the most seismically active fold-and-thrust belts all over the world. Due to large uncertainties in the location and depth of the events, earthquakes can hardly be assigned to the known active faults in the area. Coseismic surface faulting is very rare and most of the

seismicity occurs on blind reverse faults, which are buried beneath or within a faulted and folded thick sedimentary cover (Talebian & Jackson, 2004; Karasozen et al., 2019).

The Makran region, adjacent to the Zagros, is located in southeastern Iran and southern Pakistan and is part of the Eurasian-Arabian plate boundary, in which the oceanic crust of the Arabian plate in the Oman Sea from the early Cretaceous has started to subduct with a slight slope to the north beneath the Eurasian plate. The western boundary of the Makran subduction zone, which separates it from the continental collision zone of the Zagros, is defined by the Minab fault system (Maggi et al., 2002).

Regarding subduction geometry, Makran is an accretionary wedge resulting from accumulated sediments due to subduction. These sediments are gathered by the subduction of the oceanic crust and transported to the subduction boundary. The convergence rate along the Makran subduction zone is estimated to be about 2 cm per year, increasing slightly from west to east. In western and central Makran, seismicity is low, which has led to discussions about whether the deformation process in this area is locked or is aseismic (Zarifi, 2006).

Seismicity in the Zagros and Makran Transition Zone (ZMTZ) is severe due to active and dense fault systems in this region, even compared to the Zagros, which is a very active region in terms of seismicity. Moving towards Makran, the seismic activity decreases significantly. Except for significant activities on the fault system of Minab-Zendan, no other significant activity is seen on the Makran side of the transition zone. Although the depth of earthquakes is not entirely reliable due to insufficient coverage of the seismic network, the presence of deep events in the northern parts of

ZMTZ confirms the depth penetration of the subduction front with a relatively low slope.

The transition zone between the Zagros and Makran is the confluence of these two crucial seismotectonic provinces and has been considered in studies on stress in Iran (Purbeyranvand and Tatar, 2014; Ghorbani Rostam et al., 2017). This region has always been a place of arising various questions due to apparent differences in the direction of fault trends and the contrast in the amount of seismicity on disparate sides of the Strait of Hormuz.

In Figure (1), the earthquake focal mechanism data, which is used in the present study and the GPS velocity vectors, are plotted (Le Pichon & Kreemer 2010).

3. Extraction of Maximum Horizontal Stress Directions from Single Focal Mechanism Data

In addition to simple faulting regimes, including normal faulting (NF), thrust or reverse faulting (TF) and strike-slip faulting (SS), transtension or combinations of normal faulting with strike-slip faulting (NS) and thrust transpression or combination of normal faulting with strike-slip faulting (TS) are also introduced (Zoback, 1992). These are defined based on the classification of the five different tectonic stress regimes and the related orientations of the principal stress axes (Heidbach et al., 2018).

The plunges of the P, B and T axes are used to determine the σ_1 or maximum stress direction concerning the specific stress regime, as shown in Table (1) (Zoback, 1992).

4. Earthquake Focal Mechanism Data

The earthquake focal mechanism data for the study area obtained through several different sources are plotted in Figure (2). It can be seen that most of the events, as expected, are reverse or

Table 1. Determination of σ_1 directions from P, T and B axes orientations based on different tectonic Stress Regimes. P, T and B axes of the earthquake focal mechanism are compressional, extensional and null axes respectively.

P/S1-Axis	B/S2-Axis	T/S3-Axis	Regime	SH-Azimuth
$pl > 52$	$pl > 45$	$pl < 35$	NF	Azim. of B-Axis
$40 < pl < 52$	$pl > 45$	$pl < 20$	NS	Azim. of T-Axis + 90
$pl < 40$		$pl < 20$	SS	Azim. of T-Axis + 90
$pl < 20$		$pl < 40$	SS	Azim. of P-Axis
$pl < 20$		$40 < pl < 52$	TS	Azim. of P-Axis
$pl < 35$		$pl > 52$	TF	Azim. of P-Axis

strike-slip, which indicates the transpressional tectonic environment prevailing in the region. Unexpectedly, some normal mechanisms can also be observed in the study area, which is probably

caused by local extensional tectonic regimes created in the interaction between blocks or folds.

The sources from which the earthquake focal mechanisms are collected include the GCMT

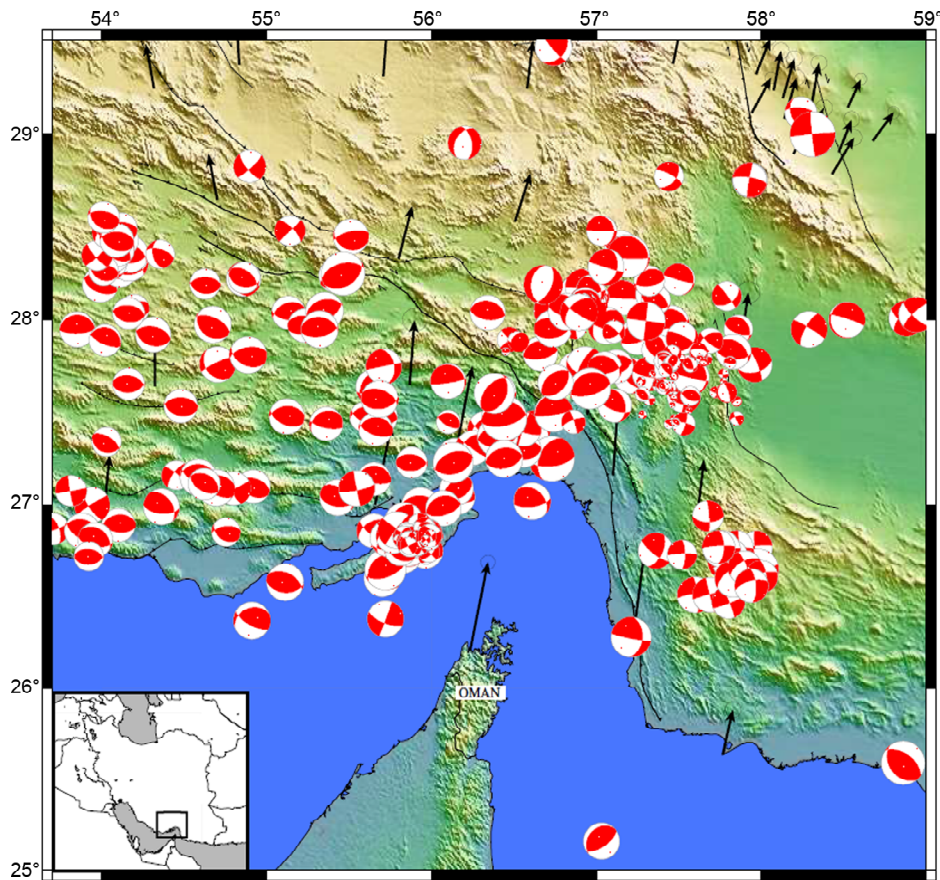


Figure 1. Map of the study area, including the focal mechanisms used in this study taken from various references (Azadfar & Gheitanchi, 2013; Gholamzadeh et al., 2009; Rezayi Nayeh, 2011; Tatar et al., 2004; Yamini-Fard et al., 2007; Yamini-Fard et al., 2006; GCMT; IRSC; ISC; NEIC; ZUR_RMT) in addition to GPS velocity vectors from (Khorrami et al., 2019).

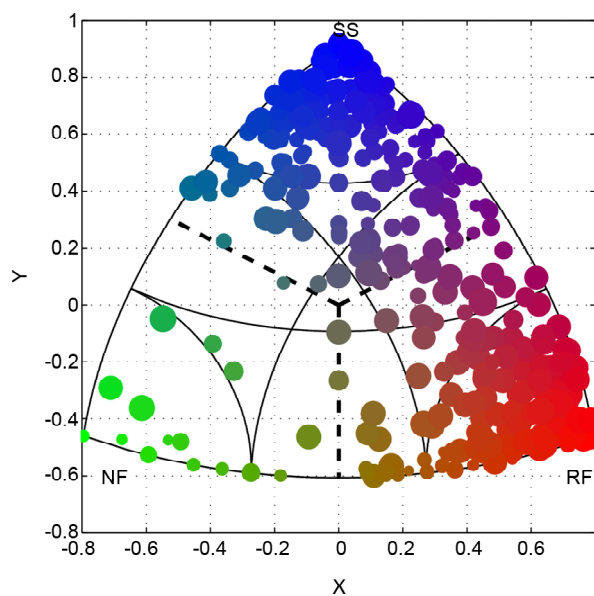


Figure 2. Kagan's triangular diagram shows the faulting mechanisms. The faulting mechanism is indicated by the color of the circles: Red is for pure reverse, green is for pure normal and blue is for pure strike-slip mechanisms.

website (formerly abbreviated HRVD), the International Seismological Center (ISC) website, the US National Earthquake Information Center website (NEIC), the website of the Swiss Seismological Service ZUR_RMT and the website of the Seismological Center of the Institute of Geophysics, University of Tehran (IRSC). Numerous articles were also used to complete the data set (Tatar et al., 2004; Gholamzadeh et al., 2009; Yamini-Fard et al., 2007; Yamini-Fard et al., 2012; Rezayi Nayeh, 2011; Azadfar and Gheitanchi, 2013; Reza et al., 2014). The focal mechanism data used in this study is obtained from the above sources during 1970 to 2020 time window.

Therefore, the resources of the compiled database consist of teleseismic and local data and the results published from local networks in scientific articles. Concerning the errors in the data and their possible influence on the results, it should be noted that the uncertainty in the focal mechanism parameters is estimated to be about 15 to 20 degrees (Hardebeck and Hauksson, 2001).

5. Introducing a New Method for Visualizing the Direction of Vector Data

The first solution to this problem, i.e., showing the direction by a color scale that one may think of, is assigning RGB combinations in different directions. But if you simply increase one, two or three values of RGB, the result is not satisfying because the color contrast between 0 and 359, which should be very little according to the definition mentioned above of the bidirectional vectors, will be the highest value that is apparently false. On the other hand, the color of each direction and its neighbor, which is the same angle +180 degrees, should be the same. This makes the problem a bit more challenging and totally differentiates the problem and solution with the case of unidirectional vectors and the color wheel. To clarify the issue, we need to go through the detail of the RGB combinations of the color wheel and the proposed new circle with central symmetry in colors, which we will call the color half circle or color wheel type 2 afterward. We will discuss the details of these issues in the following sections.

The color circle, introduced in relevant references,

is shown in Figure (3). As it can be seen, the RGB combination to create this color circle is so that every direction (or direction interval, more precisely) is represented by a unique color.

The RGB combination of this color wheel is as follows (Table 2):

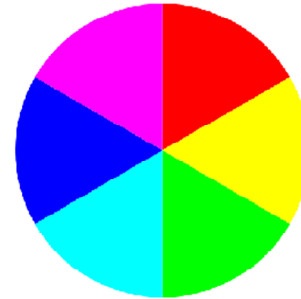


Figure 3. The usual color wheel or color circle type 1.

Table 2. RGB values for color circle type 1.

	R	G	B
0	255	0	0
60	255	255	0
120	0	255	0
180	0	255	255
240	0	0	255
300	255	0	255
360	255	0	0

If we want to show the pattern of increase and decrease in RGB values, the diagram in Figure (4) will be obtained. In this diagram, the three Red-Green-Blue value variations are shown in the upper; then, the combination can be seen in the lower part.

For the proposed new half-circle color, the circle is as follows (Figure 5).

The RGB values for this new circle are shown in Table (3).

Again, by combining the RGB values, we will have the diagrams in Figure (6).

Table 3. RGB values for color circle type 2.

	R	G	B
0	255	0	0
60	0	255	0
120	0	0	255
180	255	0	0
240	0	255	0
300	0	0	255
360	255	0	0

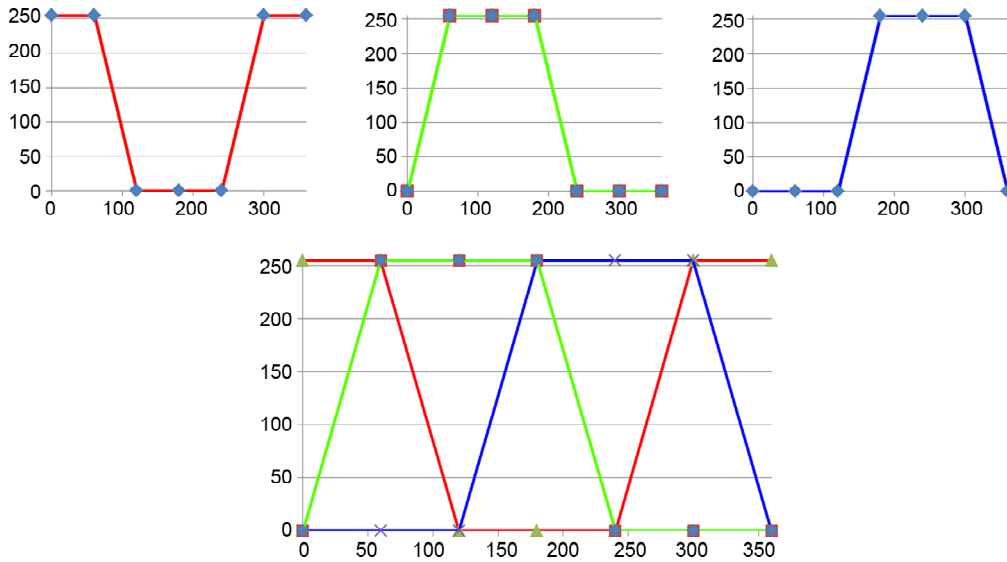


Figure 4. Diagrams showing the individual variation of RGB values (upper) and the combination of the charts (below) related to color circle type 1.

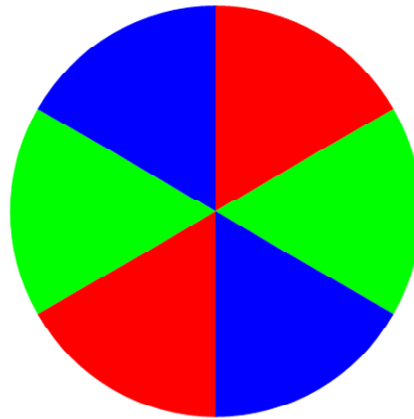


Figure 5. The proposed color wheel or the color circle type 2.

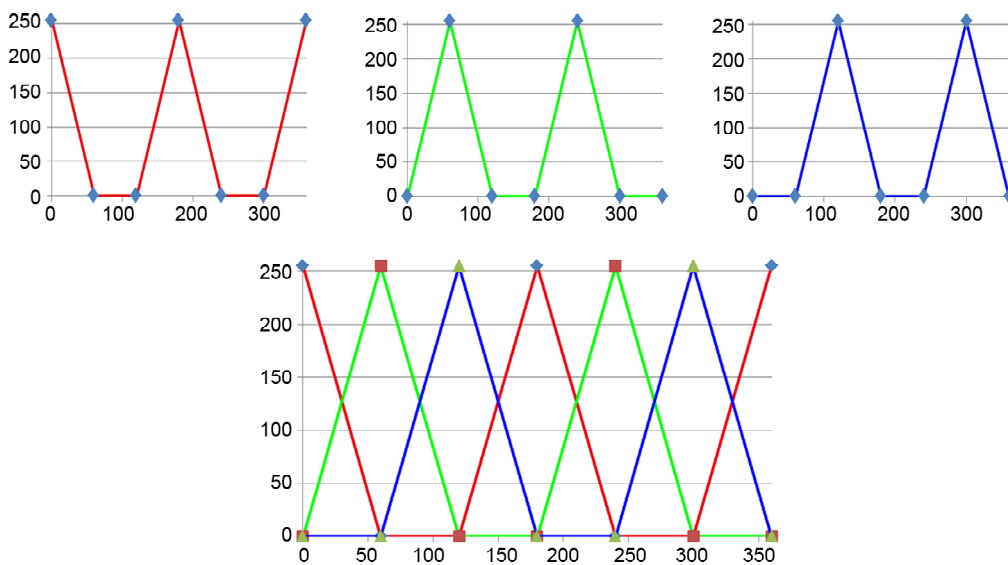


Figure 6. Diagrams showing the individual variation of RGB values (upper) and the combination of the charts (below) related to color circle type 2.

Consequently, we can further divide the whole circle and obtain finer patterns for both circles. In fact, this is how we can make the resolution of the CPT file or our color pallet higher for visualizing the direction-dependent quantity.

In Tables (4) and (5), the RGB color tables are

shown for both methods.

The created RGB color patterns can be seen in Figure (7) for 6, 12, and 24 sectors for color circles 1 and 2.

As seen in the above figure, the pattern remains constant for each color circle type; only

Table 4. RGB values for color circle type 1 with 6, 12 and 24 sectors.

	R	G	B		R	G	B		R	G	B
0	255	0	0	0	255	0	0	0	256	0	0
60	255	255	0	30	255	125	0	15	256	62	0
120	0	255	0	60	255	255	0	30	256	124	0
180	0	255	255	90	125	255	0	45	256	190	0
240	0	0	255	120	0	255	0	60	256	256	0
300	255	0	255	150	0	255	125	75	190	256	0
360	255	0	0	180	0	255	255	90	124	256	0
				210	0	125	255	105	62	256	0
				240	0	0	255	120	0	256	0
				270	125	0	255	135	0	256	62
				300	255	0	255	150	0	256	124
				330	255	0	125	165	0	256	190
				360	255	0	0	180	0	256	256
								195	0	190	256
								210	0	124	256
								225	0	62	256
								240	0	0	256
								255	62	0	256
								270	124	0	256
								285	190	0	256
								300	256	0	256
								315	256	0	190
								330	256	0	124
								345	256	0	62
								360	256	0	0

Table 5. RGB values for color circle type 2 with 6, 12 and 24 sectors.

	R	G	B		R	G	B		R	G	B
0	255	0	0	0	255	0	0	0	255	0	0
60	0	255	0	30	127	127	0	15	191	63	0
120	0	0	255	60	0	255	0	30	127	127	0
180	255	0	0	90	0	127	127	45	63	191	0
240	0	255	0	120	0	0	255	60	0	255	0
300	0	0	255	150	127	0	127	75	0	191	63
360	255	0	0	180	255	0	0	90	0	127	127
				210	127	127	0	105	0	63	191
				240	0	255	0	120	0	0	255
				270	0	127	127	135	63	0	191
				300	0	0	255	150	127	0	127
				330	127	0	127	165	191	0	63
				360	255	0	0	180	255	0	0
								195	191	63	0
								210	127	127	0
								225	63	191	0
								240	0	255	0
								255	0	191	63
								270	0	127	127
								285	0	63	191
								300	0	0	255
								315	63	0	191
								330	127	0	127
								345	191	0	63
								360	255	0	0

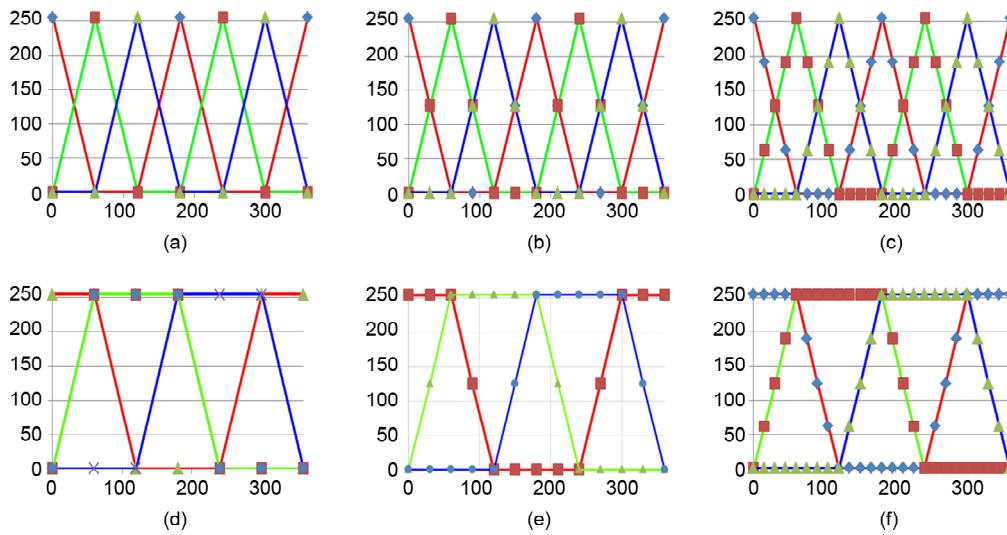


Figure 7. Diagrams showing the RGB combinations for color circle type 1 (a, b and c, respectively) and color circle type 2 (d, e and f, respectively).

the number of dots on the edges increases. In Figure (8), the resulting color circles are shown:

By continuing and further dividing the circle into more sectors, we can assign more colors to angle intervals by creating high-resolution color pallets for mapping tools like GMT. Since the RGB values used in mapping tools like GMT should be an integer, the highest possible resolution in creating CPT files to be used in these environments is limited. The resulting CPT file can reach 1536 lines at its highest for both color circle types. Thus, the highest resolution of the CPT files within this new method is achieved, but for the current dataset and color circle 2, the CPT files with 128 and 512 lines give the same image. This is because the resolution of the data we have is insufficient to

employ the full range of the visualization capacity of the proposed method. We will refer to the CPT files related to color circle 1 and color circle 2, respectively.

It should be noted that the circular color scale can not only visualize the direction of vector data but also show the magnitude of the vectors by subdividing the sectors and changing the saturation of the colors in a way that can represent the magnitude changes. Since the stress directions do not contain magnitude data, we do not need to implement the above modification in the method here.

6. Results

We use both color circle methods and check their differences for the stress or SHmax directions obtained by processing the single earthquake focal mechanism data. We implement color circle 1 or the usual color wheel for stress data available in the study area gridded by 0.2 degrees square cells. The color pallet values are assigned to each cell and interpolation is used. In other words, where the cells do not contain any data, they are filled with appropriate colors by interpolation by the proper use of GMT commands. By applying the method, Figure (9) is obtained.

It should be noted that the data have to be smoothed to give better results data when implementing this new method. Since the stress orientations are bidirectional data in the context of this study, it should be plotted by using the color

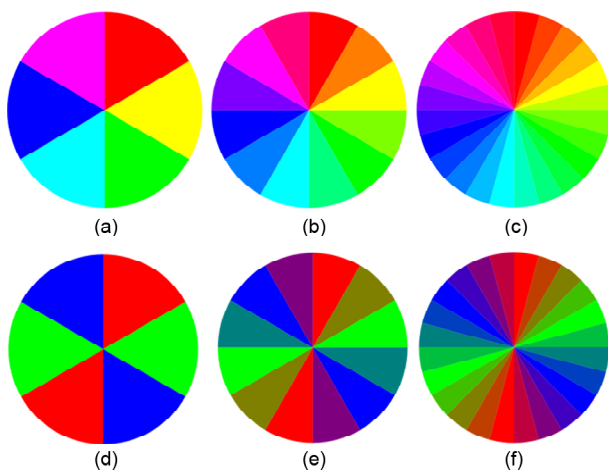


Figure 8. Color circle type 1 with 6, 12 and 24 sectors (a, b and c parts, respectively) and color circle type 2 with 6, 12 and 24 sectors (d, e and f parts, respectively).

circle type 2. However for the demonstration of the differences between the two color circles, both methods have been employed for stress data visualization in the ZMTZ area. Furthermore, the projection of the original data ranges from 0 to 360

deg. In azimuth, to 0 to 180 deg. interval can have different outputs. For a better discussion of the results, both methods are tried with and without projection to 0 to 180 deg. Figure (10) is obtained by using the data projected from 0-360 to 0-180 deg.

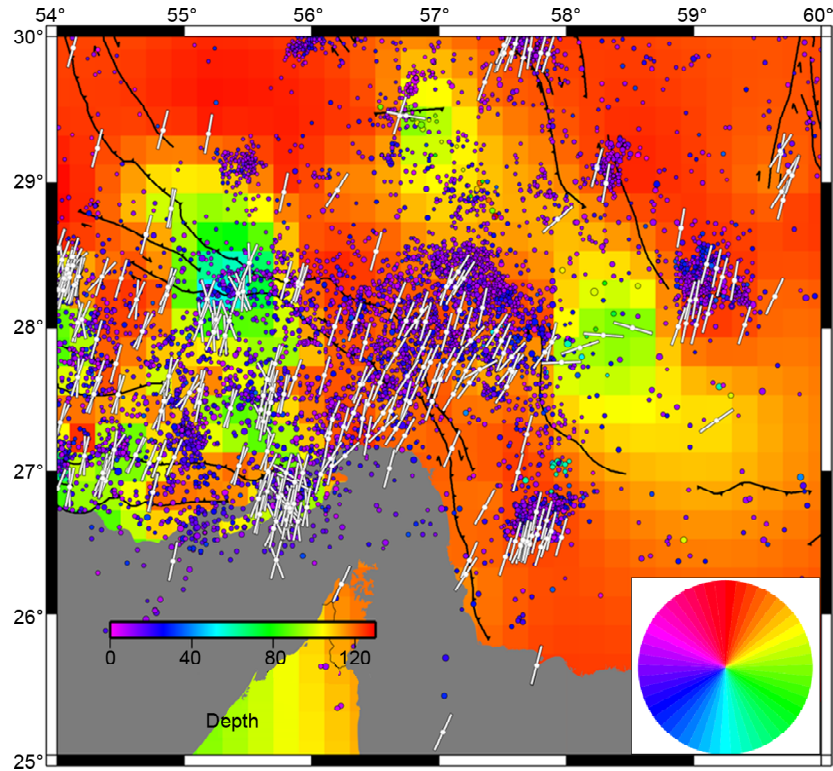


Figure 9. Stress direction mapping with color circular type 1 scale in the lower right corner.

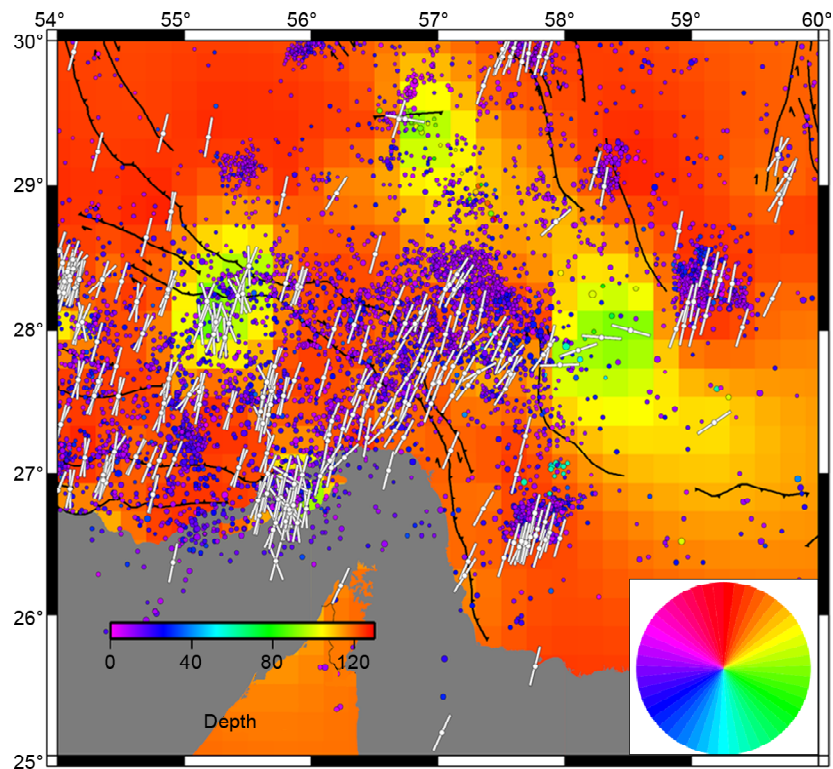


Figure 10. Stress direction mapping with color circular type 1 scale in the lower right corner.

By changing the color pallet, we obtain another view of the stress field (Figure 11).

Again by projecting the data from 0-360 deg. variation in Azimuth to 0-180, Figure (12) will be obtained.

7. Discussion

These figures contained the unseen anomalies in the stress directions and provided the first real color scaled stress maps in the study area. Comparing the above images, one can find that

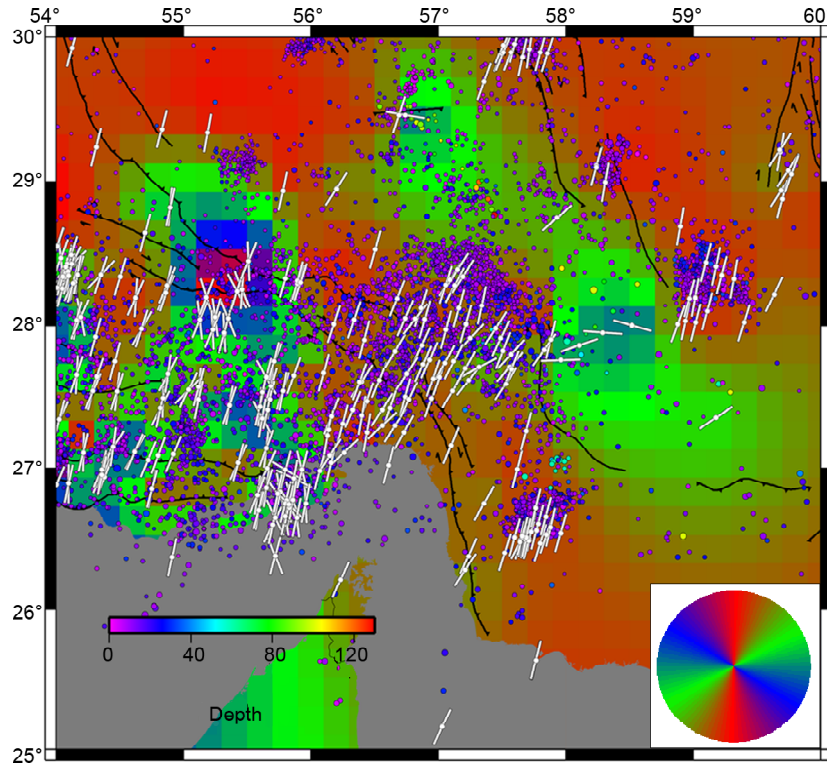


Figure 11. Stress direction mapping with color circular type 2 scale in the lower right corner.

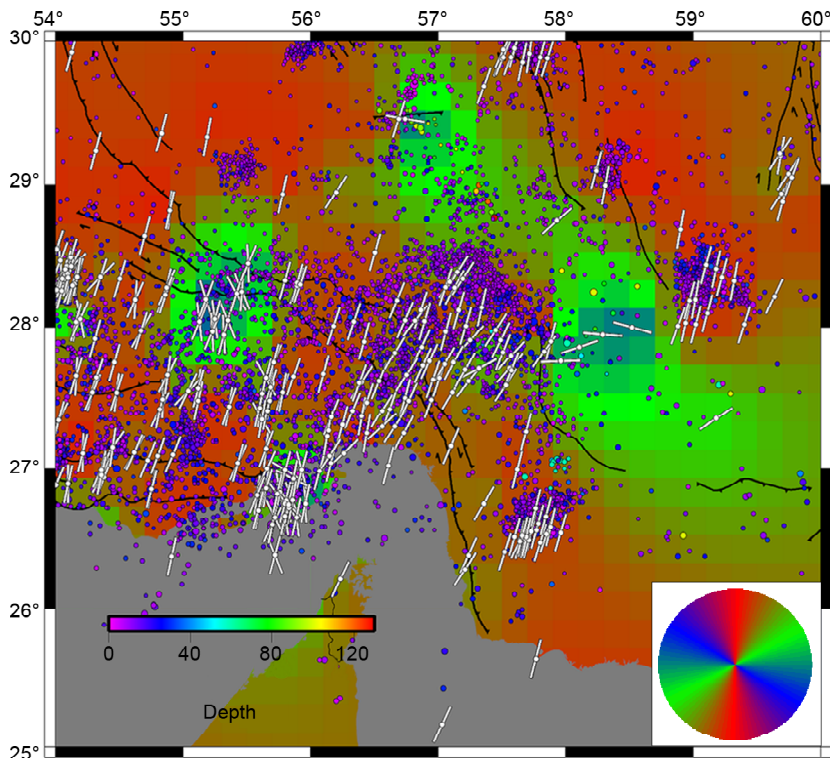


Figure 12. Stress direction mapping with color circular type 2 scale in the lower right corner (with projection to 0-180).

although the anomalies are almost identical, specific differences exist between the two images that deserve further investigation.

Concerning the projection to 0-180 deg. in Figures (10) and (12), it is evident that this mathematical manipulation simplified the maps and removes the artifacts resulting from interpolation algorithms. In other words, interpolation can cause some anomalies in the map that do not exist in the stress field, when raw data is used. But after smoothing the data, by translating azimuths between 180 and 360 degrees to the azimuths smaller than 180, the map is meaningfully more realistic and is closer to the actual stress field since it shows better agreement with the geological and tectonic facts on the ground.

The previously published results of stress studies in the area showed variations of the stress field by plotting bars in the center of the gravity of the earthquake focal mechanism clusters. But in the present study, the anomalies in the spatial variation of the stress field are illustrated for the first time. These anomalies can be interpreted according to the geology of the study area. These findings are true when looking at Figures (9) to (12).

It is obvious that according to the nature of the data under investigation, color wheel 2 should be used for visualization of the stress field and regarding the above discussion, the map with smoothed data, which is projected to 0-180 deg. is better satisfying the method criteria. Thus the final image of the stress field in the region can be described as in Figure (12).

At this point, it is worthy to note the nature of the revealed anomalies and investigate the relationship between them and the geology of the study area. There are similar anomalies in SH_{max} directions in the northeast, north and west of the Strait of Hormuz. The anomalies occur when the directions of the stress principle axes are different. Looking at Figure (12), when comparing the anomalies with the seismicity, while the depth of the events is taken into account by a separate color scale, it can be seen that anomalies in the east and north of the Strait of Hormuz occurred where the deeper events were placed. In fact, the stress direction differs in shallow and deep parts of the seismogenic zone.

It should be emphasized that this study tries to implement a new method and show its application. Possibly implementation of the method in any study area in Iran will lead to the same issues of the limitations in the data. Unfortunately, with the current database in hand, we cannot do any better. Thus, these considerations and the uncertainty in the depth of the events are emphasized, while taking in mind the need to address the weaknesses and strengths of the method by the illustration of the results by the current database. The only use of the depth of the events in the present form of the data is perhaps limited to an overall insight that distinguishes between the sedimentary cover and crystalline basement seismogenic zones, which are evident in the data with a high level of uncertainty.

Therefore, we can approximately infer that the stress field obtained from the shallow events related to the sedimentary cover differs from that of the deeper events belonging to the crystalline basement. It should be noted that the seismicity within the sedimentary cover is well explained in the technical literature related to the seismotectonic setting of the area. The Paleozoic so-called competent layer is stiffened in a way that it can form asperities to originate seismic events (Nissen et al., 2011) and that is why we observe earthquakes in the depth range equal to the thickness of the sedimentary cover, which can be up to 14 km in the area (Pirouz et al., 2017).

The anomaly to the west of the Strait of Hormuz is not accompanied by deep events as far as the limited data permits to see. Thus there should be another explanation for the observation in that part of the study area. It should be noticed then, this preliminary interpretation base on the present dataset, needs a more thorough analysis of data with a higher resolution, which can be provided by the installation and running of local seismic networks.

8. Conclusion

In the present study, in addition to the usual color circle, another color circle with central symmetry in colors is introduced and a new method in the visualization of vector data direction has been introduced. The new and unseen

anomalies in stress directions in the Zagros Makran transition zone showed significant correlations with geological and tectonic facts in the study area. Some of the anomalies coincide with deeper earthquakes. Because of the militations in the data, full interpretation of the observed anomalies need more accurate data, which can be provided by employing local seismic networks.

References

- Azadfar, M. & Gheitanchi, M. (2013). Identification of the causing fault of the 21 May 2013 Goharan earthquake using aftershock relocation and its focal mechanism. *Iranian Journal of Geophysics*, 9(4), 54-67.
- Bakhtari, H.R., Lamotte, D.F.D., Aubourg, C. & Hassanzadeh, J. (1998). Magnetic fabrics of Tertiary sandstones from the Arc of Fars (Eastern Zagros, Iran). *Tectonophysics*, 284(3-4), 299-316, doi: 10.1016/s0040-1951(97)00179-0.
- Focal Mechanism Search (n.d.). Retrieved from <http://www.isc.ac.uk/iscbulletin/search/fmechanisms>.
- Gholamzadeh, A., Yamini-Fard, F., Hessami, K. & Tatar M. (2009). The February 28, 2006, Tiab earthquake, Mw 6.0: Implications for tectonics of the transition between the Zagros continental collision and the Makran subduction zone. *Journal of Geodynamics*, 47, 280-287.
- Ghorbani Rostam, Gh., Pakzad, M., Mirzaei, N. & Sakhaei, S.R. (2017). Analysis of the stress field and strain rate in Zagros-Makran transition zone. *Journal of Seismology*, 22(1), 287-301, doi:10.1007/s10950-017-9705-x.
- Global CMT Catalog Search (GCMT) (n.d.). Retrieved from <https://www.globalcmt.org/CMTsearch.html>.
- Hardebeck, J.L. & Hauksson, E. (2001). Stress orientations obtained from earthquake focal mechanisms: What are appropriate uncertainty estimates? *Bulletin of the Seismological Society of America*, 91(2), 250-262. <https://doi.org/10.1785/0120000032>.
- Heidbach, O., Rajabi, M., Cui, X., Fuchs, K., Müller, B., Reinecker, J., Reiter, K., Tingay, M., Wenzel, F., Xie, F., Ziegler, M., Zoback, M.L. & Zoback, M. (2018). The World Stress Map database release 2016: Crustal stress pattern across scales. *Tectonophysics*, 744, 484-498, <http://doi.org/10.1016/j.tecto.2018.07.007>.
- International Seismological Centre (ISC) (n.d.). Retrieved from <http://www.isc.ac.uk/>.
- International Seismological Centre (ISC), Focal Mechanism Search (n.d.). Retrieved from <http://www.isc.ac.uk/iscbulletin/search/fmechanisms/>.
- Iranian Seismological Center (IRSC) (n.d.). Retrieved from <http://irsc.ut.ac.ir/bulletin.php>.
- Karasozen, E., Nissen, E., Bergman, E.A. & Ghods, A. (2019). Seismotectonics of the Zagros (Iran) from orogen-wide, calibrated earthquake relocations. *Journal of Geophysical Research: Solid Earth*, 124(8), 9109-9129. <https://doi.org/10.1029/2019jb017336>.
- Khorrami, F., Vernant, P., Masson, F., Nilfouroushan, F., Mousavi, Z., Nankali, H., Saadat, S.A., Walpersdorf, A., Hosseini, S., Tavakoli, P., Aghamohammadi, A. & Alijanzade, M. (2019). An up-to-date crustal deformation map of Iran using integrated campaign-mode and permanent GPS velocities. *Geophysical Journal International*, 217(2), 832-843, <https://doi.org/10.1093/gji/ggz045>.
- Le Pichon, X. & Kreemer, C. (2010). The miocene-to-present kinematic evolution of the eastern mediterranean and middle east and Its implications or dynamics. *Annu. Rev. Earth Planet. Sci.*, 38, 323-351.
- Maggi, A., Priestley, K. & Jackson, J. (2002). Focal depths of moderate to large earthquakes in Iran. *Journal of Seismology and Earthquake Engineering*, 4, 1-10.
- Masson, F., Chéry, J., Hatzfeld, D., Martinod, J., Vernant, P., Tavakoli, F. & Ghafory-Ashtiany, M. (2005). Seismic versus aseismic deformation in Iran inferred from earthquakes and geodetic data. *Geophys. J. Int.*, 160(1), 217-226.
- McQuarrie, N. (2004). Crustal scale geometry of the Zagros fold-thrust belt, Iran. *Journal of Structural Geology*, 26, 519-535.

- New Earthquake Hazards Program (NEIC) (n.d.). Retrieved from <https://www.usgs.gov/natural-hazards/earthquake-hazards/national-earthquake-information-center-neic>.
- Nissen, E., Tatar, M., Jackson, J.A. & Allen, M.B. (2011). New views on earthquake faulting in the Zagros fold-and-thrust belt of Iran. *Geophys. J. Int.*, doi: 10.1111/j.1365-246X.2011.05119.x.
- Pirouz, M., Avouac, J.-P., Gualandi, A., Hassanzadeh, J. & Sternai, P. (2017). Flexural bending of the Zagros foreland basin. *Geophysical Journal International*, 210(3), 1659-1680, DOI: 10.1093/gji/ggx252.
- Purbeyranvand, Sh. & Tatar, M. (2014). Stress variations in the Zagros using inversion of focal mechanisms of earthquakes. *Journal of Earth Sciences*, 24(94).
- Purbeyranvand, Sh. (2020). Stress field variations in the Zagros-Makran transition zone by using earthquake focal mechanism stress tensor inversion. *Iranian Journal of Geophysics*, 14(3), P. 1.
- Raeesi, M., Zarifi, Z., Nilfouroushan, F., Boroujeni, S.A., & Tiampo, K. (2016). Quantitative Analysis of Seismicity in Iran. *Pure and Applied Geophysics*, 174(3), 793-833, DOI: 10.1007/s00024-016-1435-4.
- Regard, V., Hatzfeld, D., Molinaro, M., Aubourg, C., Bayer, R., Bellier, O., Yamini-Fard, F., Peyret, M. & Abbassi, M. (2010). The transition between Makran subduction and the Zagros collision: Recent advances in its structure and active deformation. *Geological Society, London, Special Publications*, 330(1), 43-64. doi:10.1144/sp330.4.
- Reza, M., Sadidkhai, A., Abbasi, M. & Javan Doloui, Gh. (2014). Identification of the causing fault of the 29 Azar 1389 Mohammadabad Reygan earthquake (Kerman) and its focal mechanism based on aftershock analysis. *Iranian Journal of Geophysics*, 8(1), 70-59.
- Rezayi Nayeh, A. (2011). Focal Mechanism Determination Using the Relative Moment Tensor Inversion for some Earthquakes in Zarand (Iran). *M.Sc. Thesis, University of Tehran, Institute of Geophysics*, Tehran, Iran.
- Search Earthquake Catalog (n.d.). Retrieved from <https://earthquake.usgs.gov/earthquakes/search>.
- SED: Swiss Seismological Service (n.d.). Retrieved from <http://seismo.ethz.ch/en/home>.
- Shevell, S.K. (2003). *The Science of Color*. Elsevier Science, 351 pages, USA.
- Talebian, M. & Jackson, J. (2004). A reappraisal of earthquake focal mechanisms and active shortening in the Zagros mountains of Iran. *Geophys. J. Int.*, 156, 506-526.
- Tatar, M., Hatzfeld, D. & Ghafory-Ashtiany, M. (2004). Tectonics of the Central Zagros (Iran) deduced from microearthquake seismicity. *Geophys. J. Int.*, 156, 255-266.
- Vernant, P., Nilfouroushan, F., Hatzfeld, D., Abbassi, M., Vigny, C., Masson, F., Nankali, H., Martinod, J., Ashtiani, A., Bayer, R., Tavakoli, F. & Chéry, J. (2004). Contemporary crustal deformation and plate kinematics in middle east constrained by GPS measurements in Iran and Northern Oman. *Geophys. J. Int.*, 157, 381-398.
- Walpersdorf, A., Hatzfeld, D., Nankali, H., Tavakoli, F. & Nilfouroushan, F. (2006). Difference in the GPS deformation pattern of north and central Zagros (Iran). *Geophys. J. Int.*, 167, 1077-1088.
- Yamini-Fard, F., Hassanpour Sedghi, M., Gholamzadeh, A., Tatar, M. & Hessami, K. (2012). Active faulting of the Southeastern-Most Zagros (Iran): Microearthquake seismicity and crustal structure. *Journal of Geodynamics*, 55, 56-65, doi: 10.1016/j.jog.2012.01.003.
- Yamini-Fard, F., Hatzfeld, D., Tatar, M. & Mokhtari, M. (2006). Microearthquake seismicity at the intersection between the Kazerun fault and the main recent fault (Zagros, Iran). *Geophysical Journal International*, 166(1), 186-196. <https://doi.org/10.1111/j.1365-246x.2006.02891.x>
- Yamini-Fard, F., Hatzfeld, D., Farahbod, A.M. & Mokhtari, M. (2007). The diffuse transition between the Zagros continental collision and the Makran oceanic subduction (Iran): Microearthquake seismicity and crustal structure. *Geophys. J. Int.*,

170, 182-194.

Zarifi, Z. (2006). *Unusual Subduction Zones: Case Studies in Colombia and Iran*. Ph.D. Thesis, University of Bergen.

Zoback, M.L. (1992). First and second-order patterns of stress in the lithosphere: the world stress Map Project. *J. Geophys. Res.*, 97, 11703-11728, <http://doi.org/10.1029/92jb00132>.